First-principles study of the structural, energetic and electronic properties of C_{20}-carbon nanobuds

2013 Modelling Simul. Mater. Sci. Eng. 21 035006

(http://iopscience.iop.org/0965-0393/21/3/035006)

Modelling Simul. Mater. Sci. Eng. **21** (2013) 035006 (11pp) doi:10.1088/0965-0393/21/3/035006

First-principles study of the structural, energetic and electronic properties of C_{20}-carbon nanobuds

Y W Wen[1], Xiao Liu[1], Xianbao Duan[1], Rong Chen[2,4] and Bin Shan[1,3,4]

[1] State Key Laboratory of Material Processing and Die and Mould Technology and School of Materials Science and Engineering, Huazhong University of Science and Technology, Wuhan 430074, Hubei, People's Republic of China
[2] State Key Laboratory of Digital Manufacturing Equipment and Technology and School of Mechanical Science and Engineering, Huazhong University of Science and Technology, Wuhan 430074, Hubei, People's Republic of China
[3] Department of Materials Science and Engineering, The University of Texas at Dallas, Richardson, TX 75080, USA

E-mail: rongchen@mail.hust.edu.cn and bshan@mail.hust.edu.cn

Received 7 August 2012, in final form 10 January 2013
Published 21 February 2013
Online at stacks.iop.org/MSMSE/21/035006

Abstract
The structural, energetic and electronic properties of carbon nanobuds (CNBs) with the smallest fullerene C_{20} covalently attached to the sidewall of single-walled carbon nanotubes (SWNTs) are studied by first-principles calculations. Due to the high curvature of C_{20} and the resulting chemical activity, the binding between C_{20} and SWNTs is quite strong. Among different CNB configurations, bond cycloaddition is energetically most favorable. The activation barrier for C_{20}–CNB formation is only one-fourth that of C_{60} and it would maintain good stability once formed. Our results also reveal that C_{20}–CNB stability depends on the chirality of the SWNTs, and they exhibit tunable band gaps that can be modulated by the density of C_{20} attached to the SWNTs.

(Some figures may appear in colour only in the online journal)

1. Introduction

Low-dimensional carbon nanostructures such as buckyball fullerene C_{60}, carbon nanotubes (CNTs) as well as graphene exhibit unique electronic, magnetic and optical properties and have drawn a lot of attention in the scientific community due to their potential applications in nanoelectronics, gas storage and sensors [1–8]. In the past decade, ongoing efforts have been made to fabricate hybrid carbon nanostructures in order to seek new materials that may combine the advantages of individual components. The carbon nanopeapod is the first

[4] Authors to whom any correspondence should be addressed.

type of such hybrid carbon nanostructures experimentally fabricated by inserting a chain of C_{60} buckyballs inside a single-walled carbon nanotube (SWNT) [9–11]. Recently, another hybrid nanostructure called carbon nanobuds (CNBs) has been successfully synthesized with fullerenes covalently bonding to the sidewall of SWNTs [12, 13], and Raman spectroscopy in combination with transmission electron microscopy (TEM) studies provided concrete evidence for the co-existence of SWNTs and fullerenes [14]. Raman features of C_{60}–CNB have been theoretically investigated to compare them with experimental measurements and the result has indicated that the synthesized CNBs consist of C_{60} attaching to the sidewall of SWNTs [15]. Later *in situ* high resolution transmission electron microscopy (HRTEM) observations further show that CNBs can be transformed into nanopeapods by fullerene fusion and ejection into SWNTs under electron irradiation [16]. A number of studies demonstrate that CNBs have potential applications in field-emission devices [12, 13, 17, 18], hydrogen storage [19–21] and spintronics [22, 23]. Most recently, CNBs have been found to be very active when functionalized via chemical modification methods, and their transport characteristics can be used for sensor applications [24].

Despite the promising applications of CNB, the fundamental understanding of their electronic structures is still limited. For example, it was first discovered experimentally that the field emission threshold of CNBs was shifted to lower voltages compared to pristine SWNTs and the origin of the phenomena had been attributed to an effective work function (WF) decrease [12, 13]. However, later theoretical studies suggested that, contrary to experimental suggestions, a higher field emission threshold is required for CNBs and that the observed promotional effect in field emission might be due to the presence of water vapor during experiments, rather than a decrease in its intrinsic WF [17, 19]. Such theoretical investigations could help not only to clarify the origin of the observed electronic structure changes in complex hybrid structures, but also to design new carbon nanostructures better suited for specific applications. Recent examples include theoretical exploration of the porous network structure formed out of C_{60}-attached graphene CNBs with large surface areas ($\sim$2346 $m^2\ g^{-1}$) for hydrogen storage applications [20], and hydrogen storage enhancement due to the encapsulation of H_2 molecules inside fullerenes and the alternative charge distribution near the orifice [21]. However, while C_{60} is known to be the most abundant species in the fullerene family, theoretical studies indicate that the barriers of C_{60} covalently bonding to graphene is energetically unfavorable and the formation barrier is around 3.5 eV [20]. The high activation barrier for C_{60}–CNB formation implies that the rate of formation is relatively low and its existence might not be thermodynamically stable.

It is well known that the C_{20} cage is the smallest fullerene with a diameter of about 4 Å, and it is chemically active due to its highly curved surface. Such cage-structured C_{20} fullerenes have been successfully synthesized by chemical reactions from dodecahedrane $C_{20}H_{20}$ [25]. Since the diameter of C_{20} is limited, the C_{20} molecule is expected to attach onto the sidewall of an SWNT with a much smaller energy penalty. It is also worth noting that the presence of the smallest dodecahedron C_{20} fullerenes attached CNBs has been confirmed in experiments by statistical measurements of the spherical cages' size distribution on the surface of SWNTs [12]. It is thus of great interest to investigate the structural and electronic properties of C_{20}–CNBs. And to the best of our knowledge, the influence of the diameter and chirality of SWNTs to the properties of CNBs has not been investigated previously. We report here a first-principles study of the structural, energetic and electronic properties of C_{20}–CNBs with different diameters and chirality SWNTs. It is found that cycloadditions of C_{20} onto SWNTs is much easier than that of C_{60}. Among different cycloadditions, C_{20} prefers binding to SWNTs with bond-to-bond cycloaddition configuration. With respect to diameters and chiralities, the binding energies of CNBs show clear dependence on both factors of SWNTs. The minimum energy path (MEP) of

C_{20}–CNB formation shows that the energy barrier can be as low as 0.6 eV, compared with ∼3.5 eV for the C_{60}–graphene complex and ∼2.5 eV for C_{60}–CNBs [19, 20]. Electronic structure change accompanies the C_{20} adsorption, where small diameter metallic SWNTs transform into semiconductors with tunable band gaps that are modulated by the density of adsorbed C_{20} cages.

2. Computational method

Our calculations are performed using a plane-wave pseudopotential method [26–28] as implemented in the Vienna Ab-initio Simulation Package (VASP). The exchange-correlation energy is in the form of Perdew-Wang-91 [29] with generalized gradient corrections (GGA). The cutoff energy is set to 286 eV in the present calculation, which is tested to give good convergence. We adopt a standard supercell geometry structure where the tubes are aligned in a tetragonal array. The closest distance between the adjacent CNBs is set to 36 Å to eliminate the spurious periodic image interactions between CNBs in two neighboring cells. Along the tube axis, we use three unit cells for zigzag CNBs and five unit cells for armchair CNBs to avoid the periodic image interaction between C_{20} fullerenes. The $\boldsymbol{K}$-points in the Brillouin zone are sampled on a uniform grid of $1 \times 1 \times 7$ along the tube axis. All atomic positions are optimized until the magnitude of the forces acting on each atom become less than 0.05 eV $Å^{-1}$.

3. Results and discussion

C_{20} fullerene is the smallest carbon cage with a regular dodecahedron configuration, which consists of twelve pentagon rings and thirty equivalent carbon–carbon bonds. When covalently bonded to the sidewall of SWNTs, several cycloaddition configurations may form according to the symmetry. Figures 1(*a*) and (*c*) show schematic ball-and-stick models for the possible cycloadditions of C_{20}-attached zigzag and armchair CNBs. First, one carbon atom of C_{20} can bond to one carbon atom of the SWNT to form a single C–C bond as A-1, which is named atom cycloaddition. It is reported that atom cycloaddition between C_{60} and the SWNT repels each other and is unstable [19]. However, our relaxed structure of the C_{20}–CNB suggests that atom cycloaddition is stable, in part due to the higher chemical reactivity of C_{20}. In addition to that, any C–C bond of C_{20} can join to two neighboring carbon atoms of the SWNT, called bond cycloadditions, and three configurations may be produced in this case: (i) bond AB connects to the C–C bond 'along' the tube circumference as AB-12, (ii) bond AB is associated with the C–C bond 'around' tube axis as AB-23, (iii) bond AB can also be related to the contrapuntal atoms of one carbon ring of the SWNT as AB-34. Moreover, one pentagon carbon ring of C_{20} may also be attached to the hexagonal carbon ring of the SWNT face to face, which is called ring cycloaddition, and the relaxed configurations shows that only four C–C bonds are formed as ABCD-1234 due to the curvature effect. It is found for all cycloadditions that the covalent bonding between C_{20} and the SWNT induces a local distortion in the junction where some carbon atoms of the SWNT are pulled outward from the outer-wall surface and the bonding is partially transformed from sp^2- to sp^3-hybridization.

To investigate the interactions between C_{20} and SWNTs, the binding energies of the cycloaddition reactions are calculated as

$$E_b = E(\text{nanobud}) - E(\text{tube}) - E(C_{20}),$$

where E(CNB), E(tube) and $E(C_{20})$ denotes the total energy of the CNB, pristine SWNT and C_{20} fullerene, respectively. More negative binding energy indicates stronger binding and higher

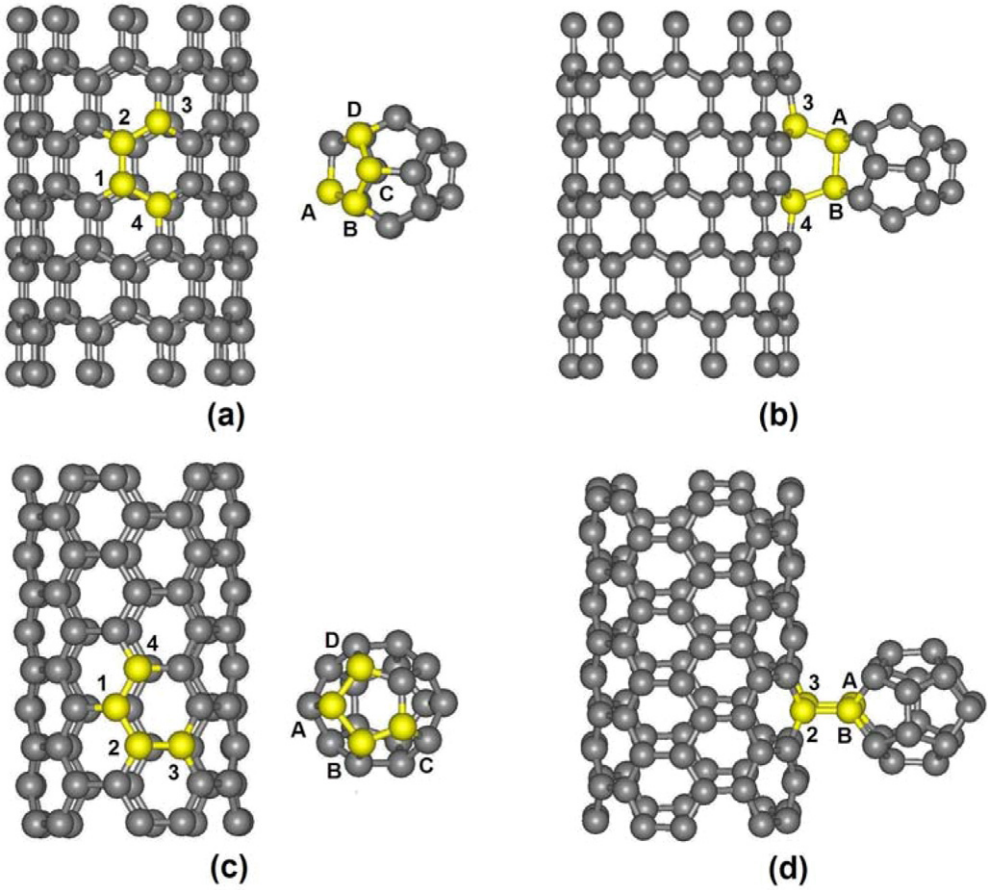

Figure 1. Schematic ball-and-stick models of possible cycloaddition sites for (*a*) (10, 0) and (*c*) (5, 5) CNB. (*b*) AB-34 and (*d*) AB-23 are the most favorable configurations for (10, 0) and (5, 5) CNB, respectively.

Table 1. Calculated binding energies (eV) of zigzag (10, 0) and armchair (5, 5) CNBs with different cycloaddition configurations.

Cycloadditions	A-1	AB-12	AB-23	AB-34	ABCD-1234
(10, 0)	–0.01	–1.03	–0.79	–1.32	0.69
(5, 5)	0.34	–0.38	–0.48	–0.22	1.72

stability of the CNB. Table 1 summarizes the calculated binding energies for aforementioned configurations of a C_{20} molecule attached to (10, 0) and (5, 5) SWNTs.

We see from table 1 that the overall binding energies of C_{20}–CNBs are negative, suggesting that the formations of C_{20}–CNBs are energetically favorable. This is in contrast to the previous study's result that all cycloadditions of C_{60} onto (5, 5) are endothermic with high positive binding energies [19]. We notice that binding of the atom cycloadditions for both (10, 0) and (5, 5) are weak, but formed C_{20}–CNBs remain stable structures instead of non-bonding in C_{60}–CNBs. The unstable configurations of atom cycloadditions for C_{60}–CNBs give us a clue that such repulsion might be strong when the distance between the SWNT and the fullerene

is as short as the length of sp^3 bonds (about 1.6 Å). It is known that C_{60} fullerene exhibits a flatter curvature than C_{20} and thus such repulsion between C_{60} and the SWNT will be stronger. While it was mentioned in the prior literature that bond cycloadditions are the most stable configuration for C_{60}–CNBs and the reactions are endothermic with required energy input from 1.5 to 2.5 eV [19], our calculations show that the C_{20} bond cycloadditions reactions onto the sidewall are exothermic for both zigzag and armchair SWNTs. These differences in bond cycloaddition energies between C_{20}– and C_{60}–CNBs can be mostly attributed to their intrinsic reactivity caused by the curvature [30].

Among all the C_{20} cycloadditions, bond cycloadditions are the most favorable. The reason is that the driving force for the decrease of energy in atom cycloaddition configuration is weak since only one covalent C–C bond is formed, while the formation of four squared carbon rings for ring cycloaddition will cause too much distortion in the junction of the C_{20}–CNB. Wu and Zeng [19] revealed the existence of two types of bond cycloadditions (AB-12 and AB-23) for C_{60}–CNBs and the former type is more favorable in energy for both zigzag and armchair tubes. It was proposed that the binding energy is closely related to the length of formed C–C bond between C_{60} and SWNTs. However, we find that the formed bond lengths of C_{20}–CNBs are very close to each other in these two configurations. Moreover, another bond cycloaddition named the AB-34 configuration is examined where one C–C bond of C_{20} is associated with the contrapuntal atoms of the carbon ring in the sidewall of SWNTs (figure 1(*b*)). This type of configuration has not been discussed in previous studies for C_{60}–CNBs. In AB-34 cycloaddition, a stereo hexagonal-like carbon ring will be formed in the junction instead of a squared one and leads to a lower binding energy. Among the three bond cycloadditions of (10, 0) CNBs, it is found that the AB-34 configuration (figure 1(*b*)) shows the lowest binding energy. For the other two cycloadditions, the AB-23 configuration is less favorable than AB-12. We have also examined other C_{20} zigzag CNBs and found the same order in binding energy. Thus, it is deduced that the most stable binding geometry of C_{20} zigzag CNBs is the AB-34 bond cycloaddition configuration. The stability of the AB-34 configuration may be explained by examining the distortions of sp^3 bonds in the junction [31]. It is well known that the ideal angle for sp^3 bonds is 109.5°. When C_{20} is attached to SWNTs bond to bond, two distorted sp^3 covalent bonds will be generated and a squared carbon ring will be formed, whereas for the AB-34 configuration, the two contrapuntal atoms are pulled out slightly and the formed sp^3 bond angle ∠3AB in figure 1(*b*) is about 107.5°, very close to the ideal one. Such a configuration leads to minimal distortions of sp^3 bonds in the junction, and would be responsible for the most favorable binding energy. For AB-12 and AB-23 cycloadditions, it is found that bond 12 (or bond 23) of the SWNT has to be pulled out to accommodate the formed sp^3 bonds. It is reasonable for the pulling of bond 12 to be easier than that of bond 23 since the neighboring four C–C bonds of bond 12 are weaker than those of the latter due to the curvature effect [32]. However, stability ordering among binding configurations is different for armchair CNBs. The AB-34 configuration of (5, 5) CNBs is not as stable as the other two bond-to-bond cycloadditions, which may be attributed to the lengthening of bond AB from 1.46 to 1.68 Å by the two contrapuntal atoms of the SWNT. In addition, a stronger repulsion will be induced near the junction region where bond AB is twisted to accommodate the two atoms. On the other hand, we find that the AB-23 cycloaddition of (5, 5) CNBs as well as that of smaller ones (3, 3) or (4, 4) is more stable than AB-12, which may be attributed to the beneficial sp^3 hybridization of AB-23 caused by the large curvature. In particular for (4, 4) and (3, 3) CNBs, the cycloaddition bond 23 is broken to fit the sp^3 hybridization in the junction, which induced a large negative binding energy. The energy difference between AB-23 and AB-12 is very close for larger diameter armchair CNBs. We thus take AB-23-type cycloaddition to be the most favorable configuration for armchair CNBs (figure 1(*d*)).

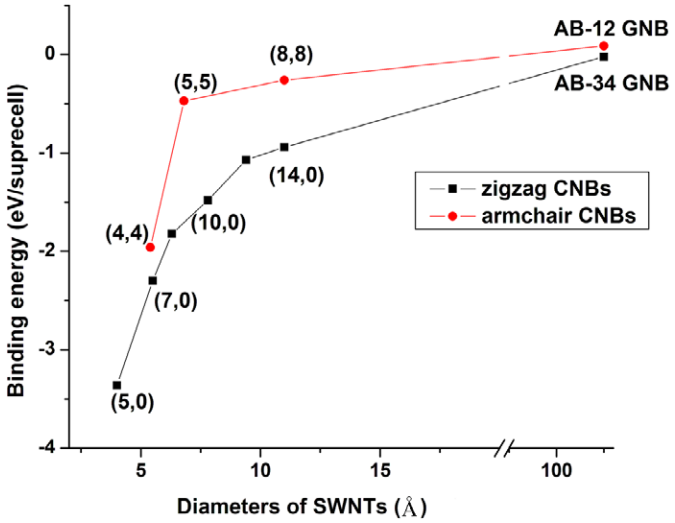

Figure 2. Binding energies of zigzag and armchair C_{20}–CNBs with different diameters.

We focus on AB-34 for zigzag CNBs and AB-23 for armchair CNBs in the following investigation of the diameter and chirality dependence of the stability of CNBs. Figure 2 gives the calculated binding energies of a series of zigzag and armchair CNBs with different diameters. Binding energies of AB-34 and AB-23 graphene nanobuds (GNBs) are also calculated to represent the binding to an SWNT in the large diameter limit.

We see that the binding energies for C_{20}–CNBs are remarkably lower, compared to the most favorable cases of the C_{60}-attached (5, 5) and (10, 0) CNBs (+1.46 and +1.56 eV per supercell). Due to a stronger curvature, the cycloadditions of C_{20} onto zigzag and armchair CNBs are all exothermic, which show much more stability than C_{60}–CNBs. Additional information can be obtained from the two curves in figure 2. Firstly, whether the C_{20} is attached to zigzag or armchair SWNTs, the binding energies monotonically increase with an increase in the SWNT diameter, which can be attributed to the curvature effects. As is known, the sidewalls of SWNTs become flatter as their diameters increase, which will lead to larger distortion of the formed sp^3 bonds and the repulsion between the C_{20} and the SWNT. If the diameter is large enough, the binding energy will approach that of GNBs. We can see that the binding energies of AB-34 and AB-23 GNBs are very close to each other, which suggest that binding energy difference between zigzag and armchair CNBs will diminish as their diameters increase. Moreover, the upper limit of the binding energies is still much lower than that of C_{60} graphene CNBs (+3.5 eV) [20]. Secondly, if we focus on (8, 8) and (14, 0) CNBs (or (5, 5) and (10, 0) CNBs), which have the same diameter but different chiralities, binding energies for zigzag CNBs are lower than armchair ones. This implies that the zigzag C_{20}–CNBs would be more stable than armchair ones with similar diameters, which are related to the detailed atomistic geometric configurations in the junction region. We note that the C_{20} molecules can also aggregate into dimers and the binding energies are comparable to those of CNBs as reported by Choi and Lee [33]. However, both the observation of C_{20}–CNBs in experiments and the relative high dissociation barrier discussed below suggest the C_{20}–CNBs do exist and should be stable once formed. We can achieve the CNB formation using techniques such as sputtering C_{20} onto CNTs to decrease the possibility of inter-collision and aggregate formation.

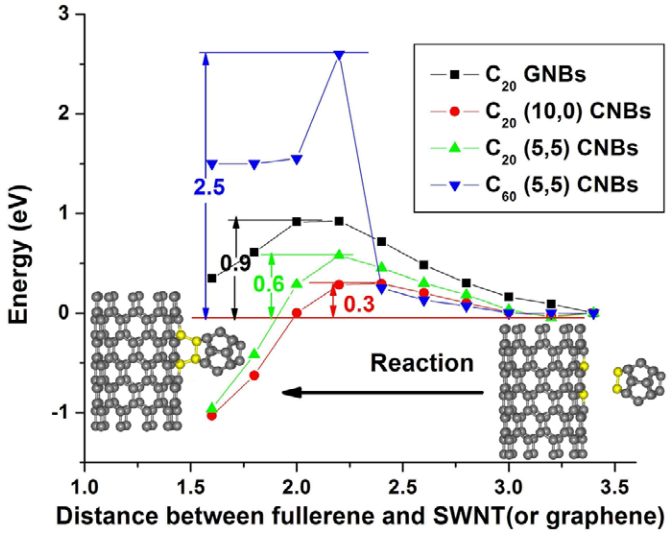

Figure 3. Estimated MEP for the formations of C_{20} (5, 5), (10, 0) CNBs and GNBs. The barrier of C_{60} (5, 5) CNBs (blue curve) is also presented from [19] for comparison.

To estimate the energy barriers of CNB formation, the MEP of C_{20}–CNB formation is calculated by a drag-and-drop method instead of a nudged elastic band (NEB) calculation, which is too time-consuming to be practical for CNBs with about 200 atoms. In our calculations, the reaction coordinate is taken to be the distance between C_{20} and CNTs. Eight intermediate images of the C_{20}-attached SWNTs are interpolated linearly between the initial state (physisorption state) and the final state (nanobuds), with the coordinates of the carbon atoms of C_{20} closest to the nanotube kept fixed at the interpolated value, and all other degrees of freedom are allowed to relax. Since the reaction path of attaching the C_{20} to the nanotube is relatively straightforward and the energy potential surface is smooth, the drag-and-drop approximation is reasonable and gives reliable results. In the case of an ultra-small diameter SWNT such as (5, 0), no stable physisorption state of a C_{20}-attached SWNT can be found, and the CNB would form spontaneously due to the intense curvatures of both C_{20} and (5, 0). For larger diameter CNBs, both stable physisorption states and chemisorptions states for CNBs exist. The MEP of C_{20} adsorbed onto zigzag (10, 0) and armchair (5, 5) SWNTs as well as graphene are plotted in figure 3 to compare with the case of C_{60}–CNBs [19].

Along the reaction coordinate which roughly corresponds to the distance between C_{20} and the SWNT, an energy barrier will be encountered as C_{20} approaches the larger diameter SWNT. It was reported that the energy barrier of C_{60} onto (5, 5) SWNTs was as high as 2.5 eV [19]. Our results reveal that a much lower barrier of 0.6 eV should be overcome along the same reaction path for C_{20} due to a stronger curvature, whereas the zigzag (10, 0) CNB with a similar diameter has a even lower barrier (0.3 eV) during the C_{20} attaching process. Such considerable barrier difference indicates that the zigzag CNBs might be preferentially formed compared to the armchair ones. The MEP of C_{20} GNBs is also calculated and plotted as a reference. The energy barrier is about 0.9 eV, which is only one-fourth that of C_{60} (3.5 eV) [20]. This serves as the upper limit kinetic barrier for the formation of C_{20}–CNBs and the low barriers give indirect evidence of the observation of C_{20}–CNBs in the experiment [12]. On the other hand, we see that the desorption barrier of C_{60} away from (5, 5) is about 1.0 eV while the desorption barrier of the C_{20}–CNB is 1.6 eV [20], suggesting that the C_{20}–CNB is more chemically stable than the C_{60}–CNB once formed.

Table 2. Number of electrons transferred from C_{20} to SWNTs (e^-); negative value means electrons transfer from SWNTs to C_{20}.

SWNT	(5, 0)	(8, 0)	(12, 0)	Graphene	(5, 5)
Charge transfer	0.058	0.015	–0.033	–0.043	–0.09

Charge transfers of CNBs are also analyzed to further investigate the interaction between C_{20} and SWNTs. Bader charge analysis [34–36] is performed to determine charge distribution quantitatively, and the transferred charge from C_{20} to SWNTs is summarized in table 2. To consider the diameter effect, charge transfer from C_{20} to graphene is also presented.

It can be seen in table 2 that charge transfers from C_{20} to ultra-small diameter zigzag SWNTs, while the other SWNTs as well as graphene donate electrons to C_{20} during the CNB formation process. As long as the hybridization effect of two C–C bonds is not dramatic compared to the whole structure, the change in the charge transfer direction can be used as a qualitative indication of the SWNT WF difference. It is expected that the electron would transfer from C_{20} to the SWNT if the effective WF of pristine C_{20} is greater than that of the SWNT and vice versa. As revealed by a previous first-principles study, the WFs of ultra-small diameter zigzag SWNTs are considerably higher than those of armchair ones and they will decrease as the diameters increase [37]. Our calculations show that electrons transfer from C_{20} to zigzag SWNTs with a diameter smaller than 6.4 Å. On the other hand, the WFs of larger diameter zigzag and armchair SWNTs are very similar and approach that of graphene. It is thus reasonable that the direction of charge transfer is from SWNTs (and graphene) to C_{20}.

To investigate the change in the electronic properties of the SWNT caused by C_{20} hybridization, the band structures of C_{20}–CNBs are plotted and we see that most of the investigated CNBs show semiconducting behavior. It is found that the large diameter CNBs such as (10, 0) and (12, 0) keep their topological band structures except for the additional flat energy levels coming from C_{20}, but smaller diameter CNBs show more interesting behavior. For small diameter ones, such as (5, 0) and (5, 5), the effect of C_{20} hybridization is much more pronounced. They transform from metallic to semiconducting ones and the band gaps are closely related to the density of C_{20} outside the wall. It is known that (5, 0) SWNTs are metallic due to strong curvature [38]. However, upon one C_{20} attaching in a $1 \times 1 \times 3$ supercell with a formula of C_{20}@60C, the double-degenerate α bands crossing the Fermi level are now split due to symmetry breaking. The two bands have a gap of 0.03 eV due to sp^3 hybridization with C_{20}, as in figure 4(*a*). The strong hybridization makes the energy level of C_{20} dispersive and broadened into a wide range. While the C_{20} density increases to one in a $1 \times 1 \times 2$ supercell (C_{20}@40C), it can be seen in figure 4(*b*) that the bands of (5, 0) near the Fermi level appear to be simpler due to a double band-folding and the band gap enlarges to 0.23 eV. It is notable that the distance between neighboring C_{20} fullerenes is about 4.5 Å and the enhanced band gap may be attributed to the increased density of sp^3 hybridization. We also show the decomposed band charge density of the (5, 0) CNB C20@60C conduction band minimum (CBM) and valence band maximum (VBM) (figures 4(*e*) and (*f*)). An obvious feature of figure 1(*f*) is that the eigenstate of the CBM extends to the junction between C_{20} and the SWNT, which is in agreement with our discussion on the contributions of hybridization to band opening. Figure 4(*c*) shows the band structure for the (5, 5) CNB within one C_{20} in a $1 \times 1 \times 5$ supercell (C_{20}@100C) and it is found that the changes in the band structure are more sensitive than that of the zigzag one. The strong hybridization between C_{20} and (5, 5) causes a serious band separation near the Fermi level. The two linear bands crossing the Fermi

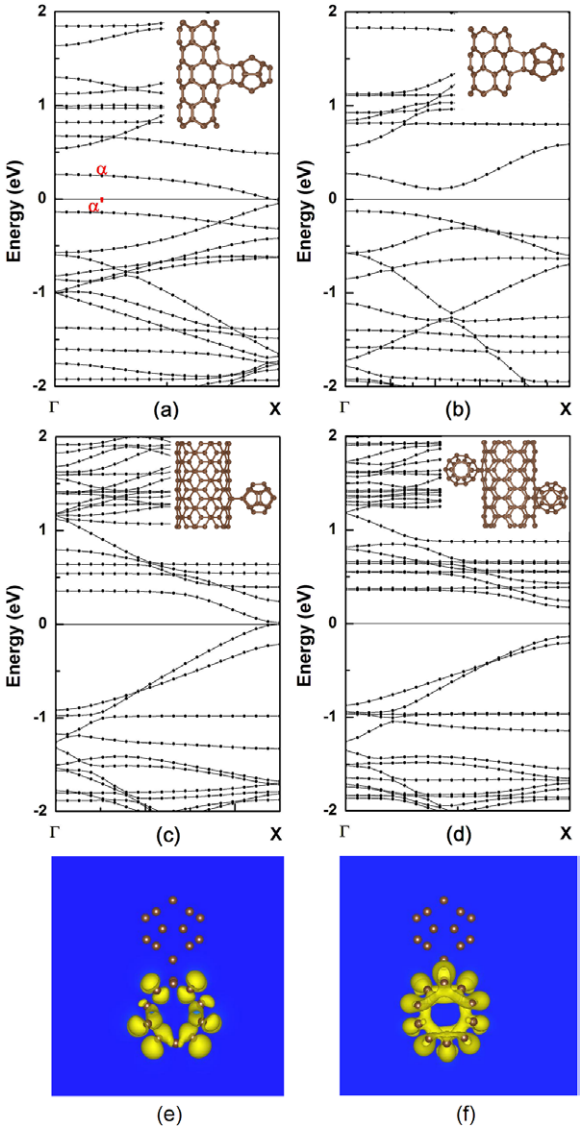

Figure 4. Band structures of CNBs with different C_{20} densities, (*a*) C_{20}@60C for (5, 0), (*b*) C_{20}@40C for (5, 0), (*c*) C_{20}@100C for (5, 5) , (*d*) C_{20}@50C for (5, 5). The insets are the corresponding unit cells of C_{20}–CNBs with different concentrations. (*e*), (*f*) are the eigenstates contours of HOMO and LUMO of (5, 0) CNBs across the formed covalent bonding, respectively.

level between Γ–X are now moving to X points due to band-folding and the intrinsic metallic crossing point at the Fermi level is now opening a gap of 0.01 eV. Again, with a higher C_{20} density of C_{20}@50C, the band gap further increases to 0.31 eV when two C_{20} fullerenes are attached to the same supercell with one on each side (figure 4(*d*)). The increased band gap with the C_{20} density is probably due to more carbon atoms transforming from sp^2 to sp^3 bonding. The change in band gaps suggests that the electronic properties of C_{20}–CNBs may be highly tunable by controlling the density of C_{20} on the sidewall of SWNTs.

4. Conclusions

We present the first-principles pseudopotential method to investigate the stability of CNB configurations where the smallest fullerene C_{20} is covalently bonded to the outside of an SWNT. It is found that the curvature and chirality of the SWNT will greatly influence the stability of C_{20}–CNBs and C_{20} would be preferentially attached to zigzag nanotubes with small diameters. The MEP of the formation of C_{20}–CNBs has lower adsorption barriers and higher desorption barriers than C_{60}–CNBs, indicating that they would be produced much more easily and would be more stable once formed. Charge transfer of CNBs is investigated and is shown to correlate closely with the WF difference between C_{20} and the SWNT. The band structure calculations show that C_{20}–CNBs exhibit semiconducting behavior and the band gaps can be tuned by controlling the density of adsorbed C_{20}.

Acknowledgments

This work is supported by the National Basic Research Program of China (2013CB934800), National Natural Science Foundation of China (11004068), Fundamental Research Funds for the Central Universities, HUST (2012TS012 and 2012TS076) and the China Postdoctoral Science Foundation (2012M521421). BS and RC would like to thank the Thousand Young Talents Plan and New Century Excellent Talents in University (NCET). The authors thank the Texas Advanced Computing Center (TACC) at The University of Texas at Austin (http://www.tacc.utexas.edu) for providing grid resources that have contributed to the research results reported within this paper.

References

[1] Kroto H W, Heath J R, O'Brien S C, Curl R F and Smalley R E 1985 *Nature* **318** 162–3
[2] Iijima S 1991 *Nature* **354** 56–8
[3] Dresselhaus M S, Dresselhaus G and Eklund P C 1996 *Science of Fullerenes and Carbon Nanotubes* (New York: Academic)
[4] Novoselov K S, Geim A K, Morozov S V, Jiang D, Zhang Y, Dubonos S V, Grigorieva I V and Firsov A A 2004 *Science* **306** 666–9
[5] Louie S G 2001 *Top. Appl. Phys.* **80** 113–45
[6] Baughman R H, Zakhidov A A and de Heer W A 2002 *Science* **297** 787–92
[7] Geim A K and Novoselov K S 2007 *Nature Mater.* **6** 183–91
[8] Geim A K and MacDonald A H 2007 Graphene: exploring carbon flatland *Physics Today* **60** 35–41
[9] Smith B W, Monthioux M and Luzzi D E 1998 *Nature* **396** 323–4
[10] Okada S, Saito S and Oshiyama A 2001 *Phys. Rev. Lett.* **86** 3835–8
[11] Lee J *et al* 2002 *Nature* **415** 1005–8
[12] Nasibulin A G *et al* 2007 *Nature Nanotechnol.* **2** 156–61
[13] Nasibulin A G, Anisimov A S, Pikhitsa P V, Jiang H, Brown D P, Choi M and Kauppinen E I 2007 *Chem. Phys. Lett.* **446** 109–14
[14] Tian Y, Chassaing D, Nasibulin A G, Ayala P, Jiang H, Anisimov A S and Kauppinen E I 2008 *J. Am. Chem. Soc.* **130** 7188–9
[15] He H Y and Pan B C 2009 *J. Phys. Chem.* C **113** 20822–6
[16] Gorantla S *et al* 2010 *Nanoscale* **2** 2077–9
[17] Meng T Z, Wang C Y and Wang S Y 2008 *Phys. Rev.* B **77** 033415
[18] Fürst J A, Hashemi J, Markussen T, Brandbyge M, Jauho A P and Nieminen R M 2009 *Phys. Rev.* B **80** 035427
[19] Wu X J and Zeng X C 2008 *ACS Nano* **2** 1459–65
[20] Wu X J and Zeng X C 2009 *Nano Lett.* **9** 250–6
[21] Wang X X, Ma C G, Chen K, Li H N and Wang P 2009 *Phys. Lett.* A **374** 87–90
[22] Zhu X and Su H B 2009 *Phys. Rev.* B **79** 165401
[23] Wang M and Li C M 2011 *Phys. Chem. Chem. Phys.* **13** 5945–51

[24] Havu P, Sillanpää A, Runeberg N, Tarus J, Seppälä E T and Nieminen R M 2012 *Phys. Rev.* B **85** 115446
[25] Prinzbach H, Weiler A, Landenberger P, Wahl F, Wörth J, Scott L T, Gelmont M, Olevano D and v. Issendorff B 2000 *Nature* **407** 60–3
[26] Kresse G and Hafner J 1993 *Phys. Rev.* B **47** 558
[27] Kresse G and Hafner J 1994 *Phys. Rev.* B **49** 14251
[28] Kresse G and Hafner J 1996 *Comput. Mater. Sci.* **6** 15–50
[29] Perdew J P and Wang Y 1992 *Phys. Rev.* B **45** 13244
[30] Park S, Srivastava D and Cho K 2003 *Nano Lett.* **3** 1273–7
[31] Sheka E F and Shaymardanova L K 2011 *J. Mater. Chem.* **21** 17128–46
[32] Wen Y W, Liu H J, Tan X J, Pan L and Shi J 2010 *J. Nanosci. Nanotechnol.* **10** 2332–5
[33] Choi C H and Lee H T 2002 *Chem. Phys. Lett.* **359** 446
[34] Henkelman G, Arnaldsson A and Jónsson H 2006 *Comput. Mater. Sci.* **36** 354–60
[35] Sanville E, Kenny S D, Smith R and Henkelman G 2007 *J. Comput. Chem.* **28** 899–908
[36] Tang W, Sanville E and Henkelman G 2009 *J. Phys.: Condens. Matter.* **21** 084204
[37] Shan B and Cho K 2005 *Phys. Rev. Lett.* **94** 236602
[38] Liu H J and Chan C T 2002 *Phys. Rev.* B **66** 115416